Effect of liquid phase on superplastic behavior of a modified 6061 aluminum alloy

R. Kaibyshev , F. Musin , D. Gromov , T.G. Nieh , D.R. Lesuer

Abstract

It is shown that a 0.15%Zr + 0.7%Cu—modified 6061 aluminum alloy with an initial grain size of about 11 μm exhibits a maximum elongation-to-failure of 1300% at 590 °C and an initial strain rate of 2.8×10^{-4} s^{-1} in a partially melted state.

Keywords: Aluminium alloys; High temperature mechanical properties; Differential thermal analysis; Incipient melting

1. Introduction

It has been established [1] that the phenomenon of high-strain-rate superplasticity (HSRS) can be related to the formation of thin, liquid-phase layers at interfaces or grain boundaries. These liquid layers result from partial melting of local areas in which the segregation of solute occurs [2]. Liquid phases play the role of a "helper" phase during the accommodation of grain boundary sliding (GBS) which results in superplastic properties [3–5]. This phenomenon has been observed in materials produced by powder metallurgy and mechanical alloying techniques [1,5]. Two important features of materials exhibiting HSRS in the partially melted state may be emphasized. First, the grain size of almost all these materials was $\leqslant 1$ μm [1]. Second, superior superplastic properties have been observed in the temperature interval from the incipient melting point, T_i, at which a small amount of liquid phase is formed to the solidus temperature, T_s, at which extensive melting begins to occur. In the temperature interval T_i–T_s no increase in the volume fraction of liquid phase takes place with increasing temperature. A small amount of liquid phase formed at T_i is present in the triple junctions and along boundaries [1].

Very little experimental results are available on the superplastic behavior of ingot-metallurgy-processed materials tested in the partially melted state. High elongation-to-failure of about 2500% has been reported only in a coarse grained (~20 μm) ingot metallurgy (IM) 7475 aluminum alloy [1]. On the other hand, it was shown that partial melting in aluminum alloys with initially coarse grain structure could result in insignificant enhancement of tensile elongation [6–8]. The role of initial

structure in the enhancement of tensile elongation due to the formation of a liquid phase and the conditions for the manifestation of superior superplastic properties by IM aluminum alloys in the partially melted state remain unclear. The aim of the present study is to report superplastic behavior in the semi-solid state of a 0.15%Zr + 0.7%Cu modified 6061 aluminum alloy produced by IM. The role of microstructure stability in the enhancement of superplastic properties in the partially melted state will be considered.

2. Experiments

The 6061 alloy with a chemical composition of Al–1.43%Mg–0.5%Si–0.7%Cu–0.15%Zr–0.26% Cr–0.14%Ti–0.17%Fe (in weight pct.) was manufactured at the Kaiser Aluminum—Center for Technology by direct chill casting. The alloy was homogenized at 530 °C for 10 h and, subsequently, a two-step thermomechanical processing (TMP) procedure was used for grain refinement.

The 6061 alloy was rolled to a 70% reduction in the temperature interval 400–250 °C, followed by recrystallization annealing at 500 °C for 30 min in a muffle furnace. Next, cold rolling with a 80% reduction was carried out, followed by final recrystallization annealing at 475 °C for 30 min in a salt bath.

Following the TMP, tensile samples with gauge lengths of 12 mm and cross-sectional areas of 5×3 mm^2 were machined parallel to the rolling direction. Tensile tests were performed at temperatures ranging from 475 to 600 °C and strain rates ranging from 7×10^{-6} to 2.8×10^{-2} s^{-1}. A computer-controlled Instron universal testing machine (Model 1185) equipped with a three-zone split furnace was used. Temperature accuracy was within ±2 °C. The values of the strain rate sensitivity, m, were determined by strain-rate-jump tests [5,9].

Differential thermal analysis (DTA) was performed in a ~19.7 mg specimen during heating to 620 °C at a rate of 10 °C min^{-1} in air by using a Rigaku analyzer (Model Thermoflex).

Samples for metallographic examinations were annealed at $T = 165$ °C for 4 h in order to decorate high angle boundaries with second phase precipitates [10]. It is known that etching in a standard Keller solution clearly outline the grain boundaries in the 6061 Al [10]. Metallographic analysis was carried out using a Neophot-32 microscope and an Epiquant automated analysis equipment. The average grain size was determined from measurements of more than 300 grains in both longitudinal and transverse directions. Cavitation was measured on the as-polished and unetched samples, using the standard point-count technique in the central area of specimens strained up to a fixed strain and in area located 5 mm from the fracture surface in specimens that have been strained to failure. For TEM examinations, samples were thinned to about 0.25 mm. Discs with 3 mm diameter were cut and electropolished to perforation with a Tenupol-3 polishing unit using a 20% nitric acid solution in methanol at −38 °C and 20 V. The thin foils were examined using a JEOL-2000EX TEM with a double-tilt stage at an accelerating potential of 160 kV. Energy dispersive X-ray analysis (EDS) of thin foils was carried out to identify second phase particles by using an Oxford attachment (Model Energy TEM200-INCA) to the Jeol-2000EX TEM and having a focused beam, with a diameter of 100 nm, which was positioned at dispersoids.

3. Results and discussion

3.1. Microstructure before deformation

The TMP resulted in the formation of uniform microstructure with an average grain size of 11.2 μm. Low angle boundaries were occasionally observed. The TEM observation has shown that the Zr addition resulted in the formation of Al_3Zr dispersoids with an average size of about 30 nm (Fig. 1a and b). It is worth noting that Al_3Zr particles were enriched by silicon. Thus, the as-processed material with a fine grain structure contains a significant volume fraction of nanoscale dispersoids which are stable at high temperatures

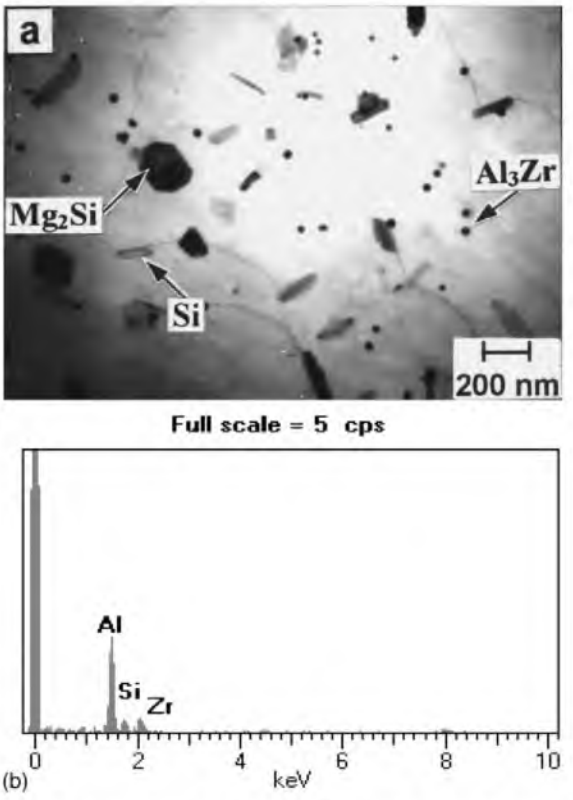

Fig. 1. Microstructure of the modified 6061 aluminum alloy: (a) TEM observation; (b) energy dispersion X-ray spectrum showing a Al_3Zr dispersoid.

and can effectively pin grain boundaries thereby providing enhanced grain stability.

3.2. Differential thermal analysis

Fig. 2 shows the DTA curve for the modified 6061 aluminum alloy. It is seen that incipient melting takes place at ~575 °C, where a weak endothermic reaction occurs. Therefore, the melting point for the present 6061 Al is 7 °C less than that for the 6061 alloy with a standard chemical composition [4,10]. Extensive melting of the present 6061 Al starts to occur at 592 °C which is the solidus temperature, T_s. Thus, the modified 6061 alloy begins to melt at $T_i = 575$ °C, and there exists the temperature interval, T_i–T_s, in which a small

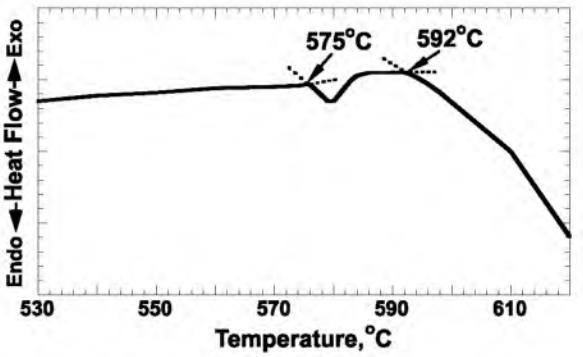

Fig. 2. DTA curve for the modified 6061 alloy. The arrows indicate the incipient melting point at 575 °C and a temperature of 592 °C at which extensive melting begins to occur.

amount of liquid phase is present in the microstructure.

3.3. Mechanical properties

Typical true stress–true strain curves for the modified 6061 aluminum alloy at fixed temperatures of 550 °C, at which the material is entirely in the solid state, and 590 °C, which is higher than T_i, are presented in Fig. 3a and b, respectively. Results are reported for strain rates ranging from 7×10^{-5} to 7×10^{-3} s^{-1}. It is seen that the σ–ε curves are essentially similar at both temperatures. At $\dot{\varepsilon} > 1.4 \times 10^{-3}$ s^{-1}, extensive strain hardening takes place initially. After reaching a maximum stress, the flow stress continuously decreases until fracture. A well defined peak in flow stress can be observed, and no steady-state flow occurs. At lower strain rates, steady-state flow can be attained. In some cases, the region of steady state flow is preceded by a softening stage. At the lower strain rates, significant secondary strain hardening takes place after steady-state flow.

The flow stress taken at a true strain of 0.4 (except at $\dot{\varepsilon} = 7 \times 10^{-3}$ s^{-1} and 590 °C, where a true strain of 0.3 was used) is plotted as a function of strain rate on a double logarithmic scale in Fig. 4a. The variation of strain rate sensitivity, m, and elongation-to-failure, δ, with strain rate are shown in Figs. 4b and 5a, respectively. A sigmoidal relationship between flow stress and strain rate, which

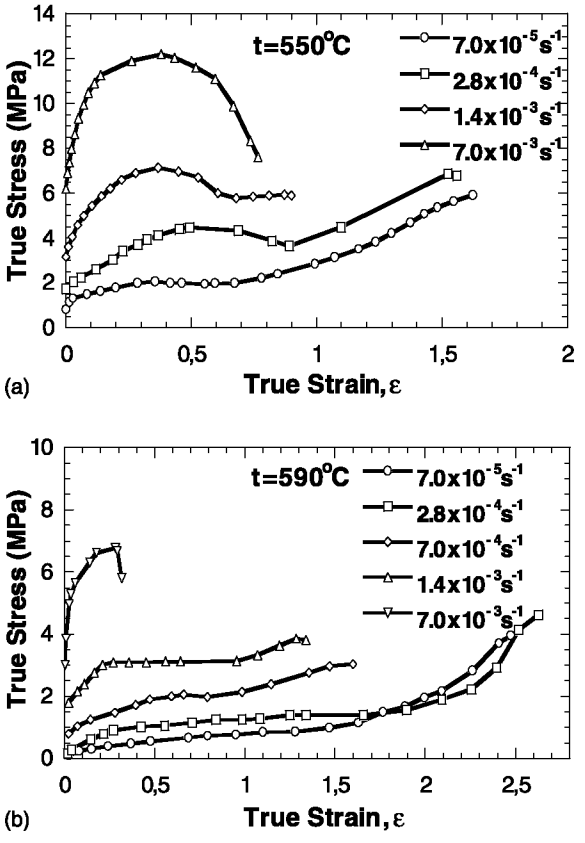

Fig. 3. Effect of strain rate on true stress–true strain curves for the 6061 Al: (a) $T = 550$ °C; (b) $T = 590$ °C.

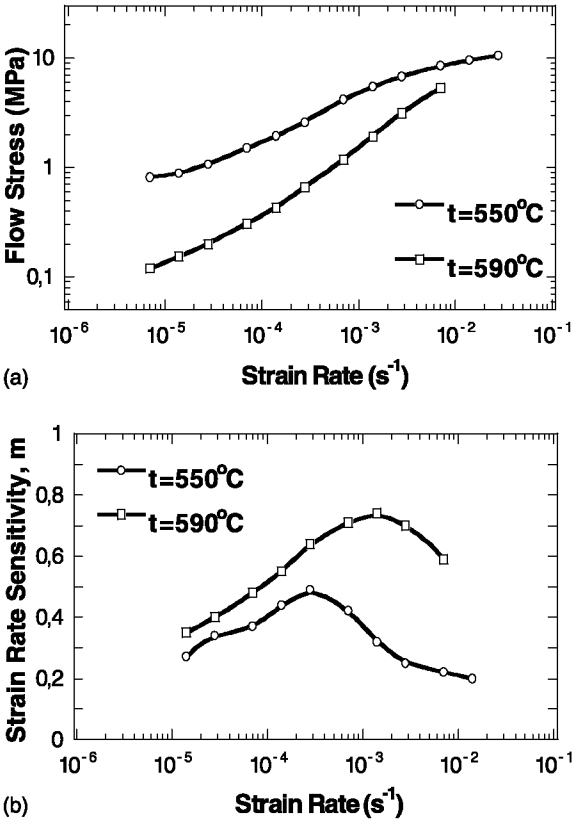

Fig. 4. Variations of flow stress, σ, (a) and coefficient of strain rate sensitivity, m, (b) with strain rate.

is typical for superplastic behavior, is observed. Three regions of superplastic deformation can be identified. The highest m values are observed in the second region. An increase in temperature from 550 to 590 °C results in a shift of the strain rate, at which the maximum value of the m coefficient is observed, from 2.8×10^{-4} to 1.4×10^{-3} s^{-1}. At 550 °C, the maximum m value is about 0.5 at $\dot{\varepsilon} = 2.8 \times 10^{-4}$ s^{-1} and elongation-to-failure is 420% at $\dot{\varepsilon} = 7 \times 10^{-5}$ s^{-1}. At 590 °C, the highest value of elongation-to-failure of 1300% takes place corresponding with $m = 0.65$ at $\dot{\varepsilon} = 2.8 \times 10^{-4}$ s^{-1}, which corresponds with $m = 0.65$. The maximum value of $m = 0.74$ was found at $\dot{\varepsilon} = 1.4 \times 10^{-3}$ s^{-1}, at which the elongation-to-failure is 280%.

With an increase in temperature, from 550 to 590 °C, the optimal strain rate region (i.e. region 2) for superplasticity, in which $m \geqslant 0.33$ [5,9], expands from 2.8×10^{-5}–1.4×10^{-3} to 1.4×10^{-5}–7×10^{-3} s^{-1}, and the optimal strain rate for superplasticity, at which maximum elongation-to-failure is observed, shifts toward higher strain rates by an order of magnitude.

At 590 °C and $\dot{\varepsilon} = 1.4 \times 10^{-5}$ s^{-1}, the m value is 0.35. With increasing strain rate up to $\dot{\varepsilon} = 1.4 \times 10^{-3}$ s^{-1}, both the m value and the elongation-to-failure increase. At $\dot{\varepsilon} \geqslant 1.4 \times 10^{-3}$ s^{-1}, a precipitous drop in the elongation-to-failure takes place with increasing strain rate. Notably, at $\dot{\varepsilon} = 7 \times 10^{-3}$ s^{-1}, the elongation-to-failure is less at 590 °C than that at 550 °C. Therefore, superplastic properties at 590 °C are superior only at strain rates lower than approximately 1.4×10^{-3} s^{-1}.

Elongation-to failure and m value as a function of temperature at $\dot{\varepsilon} = 2.8 \times 10^{-4}$ s^{-1} are plotted in

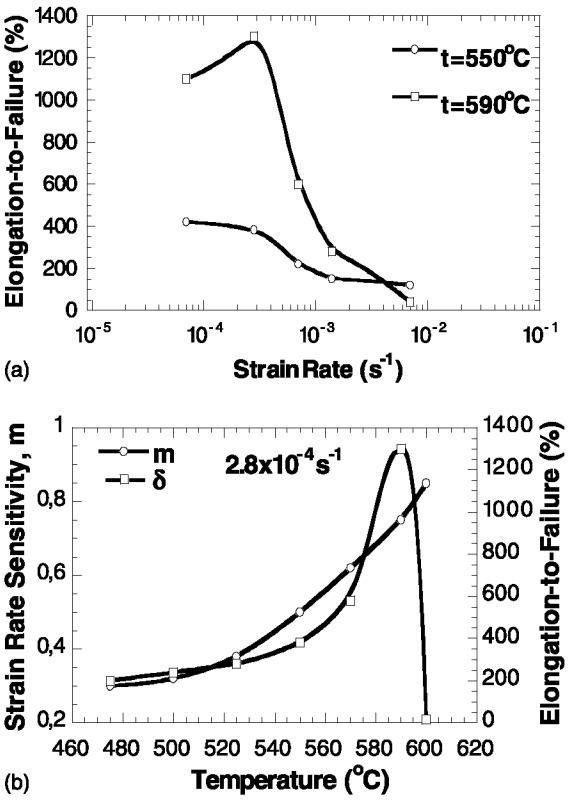

Fig. 5. Elongation-to-failure, δ, with strain rate (a); tensile elongation and m value as a function of temperature ($\dot{\varepsilon} = 2.8 \times 10^{-4}$ s^{-1}) (b).

Fig. 5b. The δ and m values tend to increase with increasing temperature in the temperature range 475–590 °C. A sharp increase in the elongation-to-failure from 580% to 1300% occurs with increasing temperature from 570 to 590 °C. The total elongation dramatically drops to 15% following the temperature increase to 600 °C, at which failure occurs at an early stage of plastic flow, in spite of the fact that the m value approaches unity (Fig. 5b), so that Newtonian viscous creep can then take place. Since the temperature of extensive melting is ~592 °C, fracture is apparently associated with the extensive formation of a liquid phase. It is likely that an increase in liquid phase volume fraction results in partial melting along grain boundaries, which can no longer support tensile force, and fracture is resulted [1].

3.4. Microstructural evolution

The microstructural evolution of the modified 6061 alloy was studied under conditions of static annealing (grip section) and superplastic deformation (i.e. dynamic annealing in the gauge section) (Table 1). Significant static grain growth at 500 °C resulted in an average grain size of about 18 μm. Further temperature increase resulted in some additional static grain growth. Notably, no significant additional grain growth occurs in the temperature interval 570–590 °C relative to 550 °C. Thus, the 6061 aluminium alloy exhibits superior superplastic characteristics in the temperature range 550–590 °C despite the fact, that the alloy has an initial structure with a relatively coarse grain size of about 20 μm.

Superplastic deformation results in grain elongation along the tension axis, and grain growth takes place in a very similar manner throughout the temperature interval 500–590 °C (AR ~ 1.24 ± 0.06). The low values of the AR can be associated with a high contribution of GBS to the total deformation [9]. Thus, at 570–590 °C, the microstructure evolves during superplastic deformation in a manner typical for deformation by GBS.

Table 1
Grain sizes observed after static annealing, L_S, and superplastic deformation at $\dot{\varepsilon} = 2.8 \times 10^{-4}$ s^{-1} to $\varepsilon = 1.1$

	T (°C)						
	475	500	525	550	570	590	600
L_S (μm)	12	17.6	18.8	20.5	21.9	21.3	26.4
L_d (μm)[a]	13.6/11.6	18/13.7	18.5/14.7	21.6/18.0	25.2/21.4	32.0/26.0	–
AR	1.17	1.3	1.26	1.2	1.18	1.23	–

L_d is the grain size after dynamic annealing, AR is the grain aspect ratio.
[a] The numerator and denominator are the grain sizes measured in the tension and transverse directions.

Table 2
Average cavity size, A, coefficient of cavity aspect ratio, CAR, and porosity volume fraction, V, for the modified 6061 alloy deformed at $\dot{\varepsilon} = 2.8 \times 10^{-4}$ s^{-1} to $\varepsilon = 1.1$

	T (°C)					
	475	500	525	550	570	590
A (μm)[a]	16.8/12.4	14.4/12.4	14.8/11.7	22.1/15.1	22.6/18.7	17.9/15.5
CAR	1.36	1.14	1.27	1.46	1.22	1.16
V (%)	0.15	0.28	0.53	0.83	1.21	0.61

[a] Numerator is the tension direction and denominator is transverse direction.

To measure cavitation during superplastic deformation in tension, specimens were strained to $\varepsilon = 1.1$ at a strain rate of 2.8×10^{-4} s^{-1} and different temperatures. The average cavity size, cavity aspect ratio, and porosity volume fraction are presented in Table 2.

At $T < T_i$, the majority of large cavities had an irregular, jagged shape (Fig. 6a). This observation suggests a plasticity-controlled cavity growth mechanism, indicating cavitation is a result of extensive GBS. In addition, the micrograph in Fig. 6a shows fine cavities exhibiting an equiaxed shape, suggesting diffusion-controlled growth of cavities during superplastic deformation. Between 500–570 °C, the cavity volume fraction and mean cavity size increase with increasing temperature (Table 2). These results could be caused by both the acceleration of diffusion processes and an increasing contribution of GBS to the total deformation with increasing temperature.

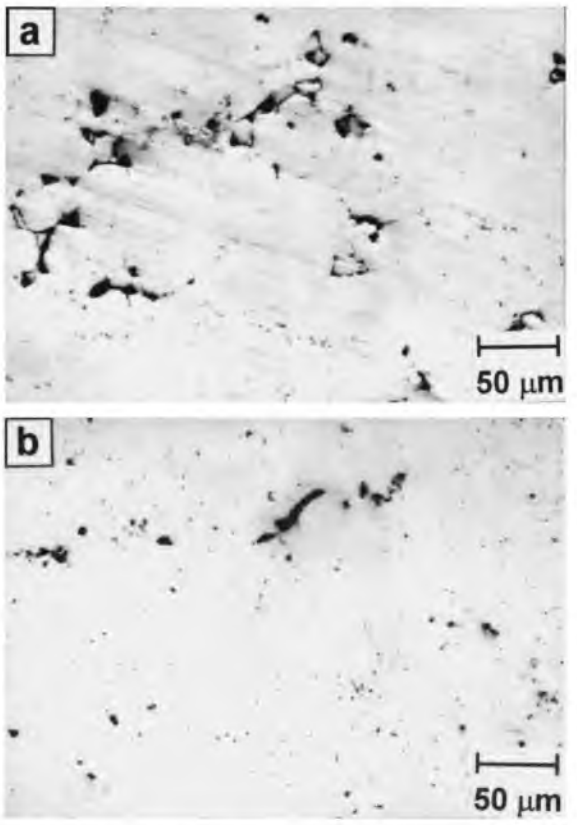

Fig. 6. Microstructure observation at $\dot{\varepsilon} = 2.8 \times 10^{-4}$ s^{-1} and $\varepsilon = 1.1$: (a) 550 °C; (b) 590 °C.

At 590 °C, the majority of cavities exhibited an equiaxed shape (Fig. 6b and Table 2). These results suggest that diffusion-controlled cavity growth dominates at 590 °C. The size of cavities and their volume fraction is less than at 570 °C (Table 2). It is apparent, that at $T > T_i$, significant GBS accommodation takes place resulting in negligible plasticity-controlled cavity growth. Thus, increasing the temperature from 570 to 590 °C resulted in a transition from plasticity-controlled cavity growth to diffusion-controlled cavity growth.

It is evident that the 0.15%Zr + 0.7%Cu—modified 6061 aluminum alloy exhibits excellent superplastic properties both in the solid state as well as in partially melted state. The superplastic behavior at temperatures below and just above the incipient melting point of ~575 °C is essentially the same. It is evident that two factors are responsible for the enhancement of superplastic properties by partial melting in the 6061 alloy. First, the high stability of microstructure (grain size ~20 μm) under static annealing and superplastic deformation in the temperature interval T_i–T_s shows that the fine Al_3Zr particles effectively restrict grain growth. The highly stable structure

is very important for manifestation of superior superplastic properties in the temperature range T_i–T_s. It is important to note that the total elongation of a commercial-grade 6061 aluminum alloy does not exceed 375% in the partially melted state due to the fact that extensive dynamic grain growth occurs [8]. Second, it is apparent that the Cu additives in the 6061 alloy result in incipient melting at ~575 °C, which is absent in the commercial grade of the 6061 alloy [4]. As a result, in the temperature interval T_i–T_s the optimum amount of liquid phase is present and the volume fraction of liquid phase remains constant with increasing temperature. At $T > T_s$, progressive melting occurs with increasing temperature and ductility decreases abruptly.

In the temperature interval T_i–T_s a significant accommodation of GBS occurs in the present 6061 alloy due to the formation of a liquid phase [1–4,6,7] providing decreased cavitation during superplastic deformation in the partially melted state.

4. Conclusion

The formation of a small amount of liquid phase may enhance superplastic properties which are exhibited by the material in the solid state. In the 0.15%Zr + 0.7%Cu—modified 6061 aluminum alloy, at $\dot{\varepsilon} = 2.8 \times 10^{-4}$ s^{-1}, the elongation-to-failure increases from 580% at 570 °C to 1300% at 590 °C due to partial melting.

Acknowledgements

This work was performed under the auspices of the US Department of Energy by the Lawrence Livermore National Laboratory under contract no. W-7405-Eng-48.

References

[1] Higashi K, Nieh TG, Mabuchi M, Wadsworth J. Scripta Metall Mater 1995;32:1079.
[2] Koike J, Mabuchi M, Higashi K. Acta Metall Mater 1995;43:199.
[3] Mabuchi M, Higashi K. Phil Mag Lett 1994;70:1.
[4] Mabuchi M, Higashi K. Mater Trans JIM 1994;35:399.
[5] Nieh TG, Wadsworth J, Sherby OD. In: Superplasticity in Metals and Ceramics. New York: Cambridge University Press; 1996. p. 210.
[6] Koike J, Miki K, Maruyama K, Oikawa H. Phil Mag A 1998;78:599.
[7] Koike J, Miki K, Takahashi H, Maruyama K. Mater Sci Eng 2000;A285:158.
[8] Nieh TG, Kaibyshev R, Musin F, Lesuer DR. Superplasticity and Superplastic Forming, TMS 1998:137.
[9] Kaibyshev OA. In: Superplasticity of Alloys, Intermetallides, and Ceramics. Berlin: Springer-Verlag; 1992. p. 316.
[10] Metallography Handbook for the Optical Metallography of Aluminum Alloys. Pleasanton, CA, USA: Kaiser Aluminum and Chemical Corporation, Center for Technology, 1992. p. 6061.6.